

Resonant three-dimensional nonlinear sloshing in a square-base basin. Part 2. Effect of higher modes

By ODD M. FALTINSEN¹, OLAV F. ROGNEBAKKE¹
AND ALEXANDER N. TIMOKHA²

¹Centre for Ships and Ocean Structures, NTNU, N-7491 Trondheim, Norway

²Friedrich-Schiller-Universität Jena, Institut für Angewandte Mathematik,
Ernst-Abbe-Platz 2-4, Jena, 07745, Germany

(Received 5 December 2003 and in revised form 13 August 2004)

The paper continues our investigations of three-dimensional nonlinear resonant fluid sloshing in a square-base basin with finite depth (mean depth/tank length ratio $h \geq 0.3$). The sloshing is forced by a combined sway/surge resonant harmonic excitation of the two lowest natural modes. The new studies are strongly motivated by a discrepancy between previous quantitative theoretical results and experimental measurements and consist of a more precise description of the strong nonlinear amplification of higher modes. The latter is justified here by secondary resonance. Effective frequency domains of the secondary resonance are quantified. An adaptive asymptotic modal theory improves agreement with earlier and new experimental data both in the transient and steady-state conditions. Local breaking and overturning near the walls, that may lead to a ‘switch’ between distinct steady regimes, increase both global damping and generate random-like excitation of higher modes, are extensively discussed.

1. Introduction

The present paper is a continuation (Part 2) of Faltinsen, Rognebakke & Timokha (2003, referred to herein) where the three-dimensional resonant fluid sloshing in a rigid square base tank was analysed by an asymptotic modal method. The tank is forced to oscillate horizontally with forcing frequency σ close to the lowest natural frequency $\sigma_{0,1} = \sigma_{1,0}$. The free-surface elevation $z = f(x, y, t)$ in the tank-fixed $Oxyz$ -coordinate system is represented as

$$f(x, y, t) = \sum_{i+j \geq 1}^{\infty} \beta_{i,j}(t) f_{i,j}(x, y), \quad (1.1)$$

where $f_{i,j}(x, y) = \cos(\pi i(x - 0.5)) \cos(\pi j(y - 0.5))$, $i + j \geq 1$ are natural modes. The unknown time-dependent modal functions $\beta_{i,j}(t)$ are ordered by introducing a small parameter ϵ characterizing the ratio between the forcing amplitude and the breadth (or length) of the tank. Faltinsen *et al.* (2000) showed by substituting (1.1) into the original non-dimensional free boundary problem or its variational analogy that such an ordering leads to a multidimensional system of ordinary differential equations coupling nonlinearly a limited set of $\beta_{i,j}$.

Those multidimensional asymptotic modal systems resemble, but are also clearly different from, a pseudo-spectral method (see Part 1). The asymptotic ordering of $\beta_{i,j}$ requires physical understanding of distinct asymptotic schemes and a quantification of frequency/amplitude domains where the order of $\beta_{i,j}(t)$ may change. Wrongly defined asymptotic ordering will lead to physically incorrect results. Part 1 used the Narimanov–Moiseyev asymptotic ordering (Narimanov 1957; Moiseyev 1958)

$$\beta_{1,0} \sim \beta_{0,1} = O(\epsilon^{1/3}), \quad \beta_{2,0} \sim \beta_{1,1} \sim \beta_{0,2} = O(\epsilon^{2/3}), \quad \beta_{i,j} \leq O(\epsilon), i + j \geq 3. \quad (1.2)$$

that had earlier been applied successfully to similar resonant sloshing problems in a vertical circular cylindrical basin. A simple system of ordinary differential equations capturing nonlinear resonant waves in the asymptotic limit $\epsilon \rightarrow 0$, $\sigma \rightarrow \sigma_{1,0}$ was derived in Part 1. The system couples nonlinearly only the nine lowest modal functions $\beta_{i,j}$, $i + j \leq 3$. Other modes are governed by linear modal equations and represent a negligible contribution. The original Moiseyev formulation assumes $|\sigma - \sigma_{1,0}| = O(\epsilon^{2/3})$. However, the derivation of this system does not assume any asymptotic relationship between $|\sigma - \sigma_{1,0}|$ and ϵ . As is accepted in asymptotic modal modelling, in contrast to traditional asymptotic schemes in fluid sloshing problems, the derivation of this system does not link $|\sigma - \sigma_{1,0}|$ and ϵ .

Possible steady solutions were classified as (i) planar (two-dimensional), (ii) diagonal or diagonal-like and (iii) swirling waves. Frequency ranges exist with no stable steady-state wave motions. Further, several stable steady solutions may co-exist. Even when ϵ was not infinitesimally small, this classification agreed well with experiments. However, a discrepancy between the theory and experiments as well as very steep surface patterns and local phenomena were found for all the three-dimensional wave regimes. We suggested that this is caused by nonlinear amplification of higher modes due to internal (secondary) resonance. The analysis of this hypothesis for steady-state and transient waves is performed in the present paper. It re-orders some modes from the set $\beta_{i,j}$, $i + j \geq 2$, to be of the same order as the dominating modal functions $\beta_{1,0}(t)$ and $\beta_{0,1}(t)$. Since the discrepancy might be due to the relatively short measurement time in the earlier experiments, new experimental results with longer durations are reported in the present paper. The main new results of Part 2 consist of:

§3.1: a modified concept of secondary resonance that quantifies frequency domains (depending on ϵ) where steady-state motions amplify some of the higher modes. This explains not only steep resonant waves, but also their selective appearance for distinct steady solutions that can co-exist;

§§3.2–3.3: an adaptive modal approach capturing both the secondary resonance and the Narimanov–Moiseyev asymptotics;

§§2.3.3: theoretical quantification of linear viscous damping rates (the papers on viscous fluid sloshing discuss the logarithmic decrements) and their influence on dominating modes;

§4: new systematic experimental results with longer time series than in Part 1. These new results are used to validate theoretical predictions of both steady-state and transient sloshing;

§4: new physical findings and limitations of modal approaches associated with more realistic prediction of damping for both dominating and non-dominating modes, ‘random-like’ dissipation and perturbations due to local phenomena.

2. Statement of the problem

Resonant sloshing in a rigid open square-base tank of breadth L_1 partially filled by a perfect fluid with mean depth h is considered. The corresponding inviscid non-dimensional formulation is presented in Part 1 (pp. 6–8). Current studies are restricted to horizontal harmonic tank motions, i.e. $\omega_i = \Psi_i = 0$, $i = 1, 2, 3$, $v_{O3} = 0$ in the notation of Part 1. The horizontal tank accelerations are defined as $\dot{v}_{Oi} = -\sigma^2 H_i \cos \sigma t$, $i = 1, 2$, where $H_1 = \epsilon \cos \theta_1$, $H_2 = \epsilon \sin \theta_2$. Here ϵ is the non-dimensional forcing amplitude and $(\cos \theta_i, \sin \theta_i)$, $i = 1, 2$ are the guiding vectors for the excitations in the Oxy -plane.

Our following analysis adopts the infinite-dimensional system of nonlinear ordinary differential equations derived in Part 1 (equation (2.15)) as an auxiliary structure in the asymptotic scheme. This system couples the full set of non-dimensional modal functions $\beta_{i,j}$, $i + j \geq 1$, and takes the following form:

$$\begin{aligned} & \ddot{\beta}^{a,b} [\delta_{ia} \delta_{jb} + d_{(a,b),(c,d)}^{1,(i,j)} \beta^{c,d} + d_{(a,b),(c,d),(e,f)}^{2,(i,j)} \beta^{c,d} \beta^{e,f}] + \sigma_{i,j}^2 \beta_{i,j} \\ & + \dot{\beta}^{a,b} \dot{\beta}^{c,d} [t_{(a,b),(c,d)}^{0,(i,j)} + t_{(a,b),(c,d),(e,f)}^{1,(i,j)} \beta^{e,f}] + P_{i,j}^{(2)} \dot{v}_{O2} + P_{i,j}^{(1)} \dot{v}_{O1} = 0, \quad i + j \geq 1, \end{aligned} \quad (2.1)$$

where the summation is performed by the repeated upper-lower indexes $i, j \geq 0$, $i + j \geq 1$. Further, $\sigma_{i,j} = \sigma_{j,i}$ are natural frequencies defined as

$$\sigma_{i,j}^2 = g \lambda_{i,j} \tanh(\lambda_{i,j} h), \quad \lambda_{i,j} = \pi \sqrt{i^2 + j^2}, \quad i, j \geq 0, \quad i + j \geq 1. \quad (2.2)$$

Expressions for $d_{(a,b),(c,d)}^{1,(i,j)}$, $d_{(a,b),(c,d),(e,f)}^{2,(i,j)}$, $t_{(a,b),(c,d)}^{0,(i,j)}$, $t_{(a,b),(c,d),(e,f)}^{1,(i,j)}$, $P_{i,j}^{(2)}$ and $S_j^{(2)}$ are given in Part 1 (pp. 36–39, $r = 1$ for square cross-section). The system (2.1) captures arbitrary progressive nonlinear activation of an infinite set of natural modes in the framework of third-order polynomial intermodal interactions; all the modes have been formally incorporated with the same order. The initial conditions

$$\beta_{i,j}(t_0) = \beta_{i,j}^0, \quad \dot{\beta}_{i,j}(t_0) = \beta_{i,j}^1, \quad i + j \geq 1 \quad (2.3)$$

with known constants $\beta_{i,j}^0$ and $\beta_{i,j}^1$ determine the initial fluid shape and initial velocity, respectively.

The infinite-dimensional model (2.1) cannot be used in numerical simulations. Further, a naive truncation of (2.1) (for instance, accounting only for $\beta_{i,j}$, $i + j \leq N$) may numerically fail or lead to physically inconsistent results (La Rocca, Mele & Armenio 1997; Faltinsen & Timokha 2001). Since this is in many cases caused by wrong intermodal ordering, an asymptotic analysis should *a priori* check for necessary nonlinearities. Damping must also be considered. One way is to incorporate the linear terms $2\alpha_{i,j} \dot{\beta}_{i,j}$ in (2.1), where $\alpha_{i,j}$ are the damping rates. Faltinsen, Rognbakke & Timokha (2004) expressed $\alpha_{i,j}$ as $\alpha_{i,j}^{\text{surface}} + \alpha_{i,j}^{\text{bulk}}$ where

$$\alpha_{i,j}^{\text{surface}} = \sqrt{\frac{v \sigma_{i,j}}{2}} \left[\frac{3}{2} + \frac{\lambda_{i,j}}{\sinh(2\lambda_{i,j} h)} \left(\frac{1}{2} - h \right) \right] \quad (2.4)$$

is due to shear stresses on the internal tank surface and

$$\alpha_{i,j}^{\text{bulk}} = 2v \left[\left(\frac{\pi^4 (ij)^2}{\lambda_{i,j}^2} + \lambda_{i,j}^2 \right) + \frac{2h}{\lambda_{i,j}} \frac{\pi^4 (ij)^2 - \lambda_{i,j}^4}{\sinh(2\lambda_{i,j} h)} \right] \quad (2.5)$$

is associated with dissipation in the fluid bulk. Here v is the non-dimensional kinematic

viscosity. Formulae (2.4) and (2.5) assume $\lambda_{i,j} = O(1)$ which is true only for a few of the lowest natural modes.

The hydrodynamic force can, based on Faltinsen *et al.* (2004), be expressed as

$$F_1 = ml_1 [-\dot{v}_{O1} - \ddot{x}_C], \quad F_2 = ml_1 [-\dot{v}_{O2} - \ddot{y}_C], \quad F_3 = ml_1 [-g_0 - \dot{v}_{O3} - \ddot{z}_C], \quad (2.6)$$

where the second derivative of the mass centre is

$$\left. \begin{aligned} \ddot{x}_C &= -\frac{1}{\pi^2 h} \sum_{i=1}^{\infty} \ddot{\beta}^{i,0} \frac{1 + (-1)^{i+1}}{i^2}, \\ \ddot{y}_C &= -\frac{1}{\pi^2 h r} \sum_{i=1}^{\infty} \ddot{\beta}^{0,i} \frac{1 + (-1)^{i+1}}{i^2}, \\ \ddot{z}_C &= \frac{1}{2h} \left[\sum_{i=1}^{\infty} [\ddot{\beta}^{i,0} \beta^{i,0} + (\dot{\beta}^{i,0})^2 + \ddot{\beta}^{0,i} \beta^{0,i} + (\dot{\beta}^{0,i})^2] + \frac{1}{2} \sum_{i,j=1}^{\infty} [\ddot{\beta}^{i,j} \beta^{i,j} + (\dot{\beta}^{i,j})^2] \right]. \end{aligned} \right\} \quad (2.7)$$

3. Resonant amplification of higher modes and an adaptive asymptotic modal approach

3.1. Secondary resonance in a square-base basin

Even if only the lowest modes $\beta_{0,1}$ and $\beta_{1,0}$ are resonantly excited, some higher natural frequencies $\sigma_{i,j}$, $i + j \geq 2$, may, due to nonlinearities, become close to combinations of forcing frequency and natural frequencies (Bryant 1989; La Rocca *et al.* 1997; Faltinsen & Timokha 2001). This causes amplification of corresponding higher modes. The occurrence of such a combinatoric (secondary) resonance in steady solutions is easily quantified for infinitesimal ϵ by analysing the nonlinear structure of the infinite-dimensional modal system (2.1). Assuming the primary resonance $\sigma \approx \sigma_{0,1} = \sigma_{1,0}$ and using a Fourier representation of periodic solutions we deduce the dominating harmonics $\cos(N\sigma t)$ and $\sin(N\sigma t)$ in $\beta_{i,j}(t)$, $i + j = N \geq 1$. The secondary resonant amplification of one of these harmonics with $i + j \geq 2$ is associated with the following two conditions:

$$\left| \frac{\sigma}{\sigma_{1,0}} - i_{i,j} \right| \ll 1, \quad \left| \frac{\sigma}{\sigma_{1,0}} - 1 \right| \ll 1, \quad (3.1)$$

to be fulfilled simultaneously with $i_{i,j} = \sigma_{i,j}/(N\sigma_{1,0})$.

The smallness in the inequalities (3.1) should be considered in an asymptotic scale depending on ϵ . Calculations based on the finite-depth dispersion relationship for $\sigma_{i,j}$ show that $i_{i,j} \neq 1$ for $i + j \geq 2$. In particular, $i_{1,1} < i_{1,1} = 0.614 \dots < i_{2,0} = i_{0,2} = 0.73 \dots$, $i + j \geq 3$ for $h = 0.5$. Conditions (3.1) can therefore only be satisfied either in the limit $h \rightarrow 0$ (shallow fluid sloshing) or for finite h as ϵ increases. This is explained by Faltinsen & Timokha (2001) (for two-dimensional sloshing in a rectangular tank): growing ϵ increases the scaling for inequalities in (3.1) so that the effective resonant frequency domains $1 - \delta_1 < \sigma/\sigma_{1,0} < 1 + \delta_1$, $i_{2,0} - \delta_2 < \sigma/\sigma_{1,0} < i_{2,0} + \delta_2$ and $i_{3,0} - \delta_3 < \sigma/\sigma_{1,0} < i_{3,0} + \delta_3$ overlap beginning from a still small, but non-infinitesimal ϵ . Two-dimensional analysis shows that the overlapped effective domain should always include the frequency range $i_{2,0} < \sigma/\sigma_{1,0} < 1$.

Experiments in Part 1 were done with finite h and relatively small ϵ . They detected amplification of the higher modes only for three-dimensional waves and only in a narrow zone around the primary resonance $\sigma/\sigma_{1,0} = 1$. Two-dimensional sloshing

phenomena were consistent with the Narimanov–Moiseyev prediction in the domain mentioned, $i_{2,0} < \sigma/\sigma_{1,0} < 1$. This means that the two previous approaches based on either an increasing ϵ or a decreasing h become inapplicable in this case. We propose an alternative approach to quantify the amplification due to the secondary resonance phenomena for steady-state motions.

The analysis of steady solutions starts with the original asymptotics

$$\frac{\sigma_{1,0}^2}{\sigma^2} - 1 = O(\epsilon^{2/3}). \quad (3.2)$$

It restricts the forcing frequency and leads to the asymptotic solution (see (3.8) from Part 1)

$$\beta_{1,0} = A \cos \sigma t + \bar{A} \sin \sigma t + o(\epsilon^{1/3}), \quad \beta_{0,1} = \bar{B} \cos \sigma t + B \sin \sigma t + o(\epsilon^{1/3}), \quad (3.3a)$$

$$\left. \begin{aligned} \beta_{2,0} &= p_0(A^2 + \bar{A}^2) + h_0(A^2 - \bar{A}^2) \cos 2\sigma t + 2h_0 A \bar{A} \sin 2\sigma t + o(\epsilon), \\ \beta_{0,2} &= p_0(\bar{B}^2 + B^2) + h_0(\bar{B}^2 - B^2) \cos 2\sigma t + 2h_0 \bar{B} B \sin 2\sigma t + o(\epsilon), \\ \beta_{1,1} &= p_1(A\bar{B} + \bar{A}B) + h_1(A\bar{B} - \bar{A}B) \cos 2\sigma t + h_1(\bar{A}\bar{B} + AB) \sin 2\sigma t + o(\epsilon), \end{aligned} \right\} \quad (3.3b)$$

where steady amplitudes A, \bar{A}, \bar{B} and B are of $O(\epsilon^{1/3})$.

The coefficients p_0 and p_1 are always of $O(1)$ while h_0 and h_1 are proportional to $1/(\sigma_{2,0}^2/\sigma^2 - 4)$ and $1/(\sigma_{1,1}^2/\sigma^2 - 4)$, respectively (see expressions on p. 13 of Part 1). This makes h_0 and h_1 infinite under the secondary resonance condition, namely when $\sigma/\sigma_{i,j} \rightarrow i_{i,j}$, $i + j = 2$. If h_0 and h_1 are still of $O(1)$, equations (3.3b) show that the second-order modal functions $\beta_{2,0}, \beta_{0,2}, \beta_{1,1}$ are formally proportional to $\|\beta_{1,0}, \beta_{0,1}\|^2$. Here $\|\beta_{1,0}, \beta_{0,1}\|$ is a norm of $\beta_{1,0}$ and $\beta_{0,1}$, which by accounting for the dominating asymptotic contribution from A, \bar{A}, \bar{B} and B can be expressed as

$$\|\beta_{1,0}, \beta_{0,1}\| = \sqrt{A^2 + \bar{A}^2 + B^2 + \bar{B}^2}. \quad (3.4)$$

Since A, \bar{A}, B, \bar{B} vary along the response curves (see figures 5–9, 11, 12 in Part 1), the magnitude of the second-order modal functions $\beta_{2,0}, \beta_{0,2}, \beta_{1,1}$ depends on the type of steady solution and $\sigma/\sigma_{0,1}$. A simple asymptotic analysis based on (3.3b) and the structure of the coefficients h_0 and h_1 , gives the following sufficient and necessary condition:

$$D_{i,j}(\sigma/\sigma_{1,0}) = \left| \left(\frac{\sigma_{i,j}}{(i+j)\sigma} \right)^2 - 1 \right| / \|\beta_{1,0}, \beta_{0,1}\| = O(1), \quad i + j = 2 \quad (3.5)$$

for steady solution (3.3b) to be comparable with the norm $\|\beta_{1,0}, \beta_{0,1}\|$. Otherwise, (1.2) and (3.2) lead to $D_{i,j} = O(\epsilon^{-1/3})$, $i + j = 2$.

Condition (3.5) depends on both the frequency domain and the type of steady-state wave motions and makes it possible to quantify secondary resonance for a fixed ϵ . We give some calculations associated with the experimental results reported below (longitudinal forcing, $h = 0.5, \epsilon = 0.00817$) in figure 1. Since $i_{2,0} = 0.73 \dots$ and $i_{1,1} = 0.614 \dots$ represent relatively close values for the asymptotic scale $\epsilon^{1/3}$, the graphs for $D_{2,0}$ and $D_{1,1}$ are almost identical and we present only results for $D_{2,0}$. Figure 1 contains three types of branches representing possible stable steady-state solutions: two sub-branches (solid lines) correspond to planar waves, the dashed line shows swirling waves and the dotted line represents stable ‘square’-like (diagonal) fluid motions. Under certain circumstances, the values of $D_{2,0}$ on the solid lines are relatively large and do not satisfy (3.5). This means that the modal system in Part 1 based on Moiseyev’s asymptotics (1.2) is applicable for planar waves. In contrast, it is

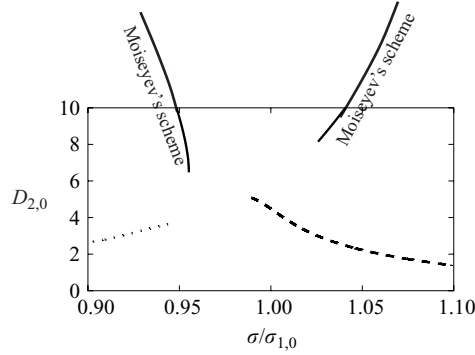


FIGURE 1. Asymptotic estimates of $D_{2,0}$ defined in (3.5) versus $\sigma/\sigma_{1,0}$ for longitudinal horizontal forcing with $\epsilon = 0.00817$ and $h = 0.5$. $D_{2,0}$ are calculated for planar (solid lines), swirling (dashed) and ‘square’-like (dotted) stable steady solutions classified in Part 1. Asymptotic condition $D_{2,0} = O(1)$ along the branches implies that the modal function $\beta_{2,0}$, $\beta_{0,2}$, $\beta_{1,1}$ should be of the order of the primary modal functions $\beta_{1,0}$ and $\beta_{0,1}$. This condition is satisfied for swirling and ‘square’-like, but not planar waves.

likely that $D_{2,0} = O(1)$ on the branch corresponding to the stable swirling and ‘square’-like waves. This implies that $\beta_{2,0}$, $\beta_{0,2}$ and $\beta_{1,1}$ ($D_{1,1} \approx D_{2,0}$ in calculations) disagree with (1.2) for these three-dimensional regimes. Since condition $D_{2,0}$, $D_{1,1} = O(1)$ leads to $\beta_{i,j} \sim \beta_{0,1} \sim \beta_{1,0}$ for $i + j = 2$, at least five modes $\beta_{i,j}$, $i + j \leq 2$, should have the same lowest order.

The asymptotic procedure quantifying possible amplification of the modes $i + j \geq 3$ can be extended recursively starting from the estimate (3.5) made for $N = 2$. A general structure of such a condition for the mode i, j takes the following form:

$$D_{i,j}(\sigma/\sigma_{1,0}) = \left| \left(\frac{\sigma_{i,j}}{(i+j)\sigma} \right)^2 - 1 \right| / \|\beta_{l,m}\| = O(1), \quad (3.6)$$

where $\|\beta_{l,m}\|$ is a new norm, which has to include contributions from all the lowest-order modal functions $\beta_{l,m}$, $l + m \leq N$. This is an analytically tedious task, even for $i + j = 3$. In this case, the derivation of explicit expressions for (3.6) needs asymptotic periodic solutions of the original free boundary problem, where the five lowest modes ($\beta_{i,j}$, $i + j \leq 2$) are of the same, dominating order. This problem could be the subject of a new publication.

3.2. Secondary resonance asymptotics

The probability for higher modes to be strongly amplified implies that the earlier scheme based on (1.2) is limited to a qualitative character for the three-dimensional waves. A new modal ordering is needed, in which some of the higher modes have the lowest order. Since quantifications of the amplification for $\beta_{i,j}$, $i + j = N$, are approximately the same for a fixed N , a selection of dominating modes can be made with the condition $i + j \leq N$.

Let us assume $N \geq 2$ and consider $\beta_{i,j}(t) = O(\epsilon^{\chi_1})$, ($\chi_1 < 1$), $i + j \leq N$ in the lowest asymptotic order. The secondary resonance condition should in a similar way as the Moiseyev detuning (3.2) satisfy the relationships $(\sigma_{i,j}/((i+j)\sigma))^2 - 1 = O(\epsilon^{\chi_2})$, ($\chi_2 < 1$). Matching the lowest-order terms in the modal system (2.1) to $O(\epsilon)$ leads to

$\chi_1 = \chi_2 = 1/2$, i.e.

$$\left. \begin{aligned} \beta_{i,j} &= O(\epsilon^{1/2}), \quad \left(\frac{\sigma_{i,j}}{(i+j)\sigma} \right)^2 - 1 = O(\epsilon^{1/2}), \quad i+j \leq N, \\ \beta_{i,j} &= O(\epsilon), \quad \left(\frac{\sigma_{i,j}}{(i+j)\sigma} \right)^2 - 1 = O(1), \quad N+1 \leq i+j \leq 2N. \end{aligned} \right\} \quad (3.7)$$

It is very important to note that (3.7) is not applicable for $N = 1$. Its usage gives in that case only a linear approximation of dominating $\beta_{0,1}$ and $\beta_{1,0}$ and the matched χ_1, χ_2 should be consistent with the Narimanov–Moiseyev ordering. Accounting for (3.7) in (2.1) and keeping terms of $O(\epsilon)$ leads to a second-order asymptotic modal system, where the third-order polynomial terms at $d_{(a,b),(c,d),(e,f)}^{2,(i,j)}$ and $t_{(a,b),(c,d),(e,f)}^{1,(i,j)}$ in (2.1) become of $o(\epsilon)$ and may be omitted. The second-order system includes nonlinearly coupled dominating modal functions $\beta_{i,j}, i+j \leq N$, while the driven modal functions $\beta_{i,j}, N+1 \leq i+j \leq 2N$, are linear themselves, but nonlinearly excited by the dominating modes.

3.3. Adaptive modal approach

Although the second-order asymptotic modal systems based on (3.7) are easily derivable, they cannot be implemented in the sloshing analysis. The first problem is that conditions (3.5) and (3.6) quantifying the number N are of asymptotic nature and the exact value of N is in practice not clearly determined. Even very small changes in forcing frequency and amplitude, or a passage to transient waves can affect N . Further, the different asymptotic assumptions for different types of waves should be captured, e.g. planar waves should be based on (1.2) while three-dimensional steady solutions require (3.7). Since the asymptotic modal system should be used for both transient and steady-state conditions, a switch between those types of wave motions must be handled. An adaptive scheme is therefore needed. In order to keep the necessary nonlinear terms in (2.1) required by both asymptotics (1.2) and (3.7), the adaptive asymptotic modal system must include the terms needed by the relationships

$$\left. \begin{aligned} \beta_{i,j} &= O(\epsilon^{1/3}), \quad i+j \leq N; \quad \beta_{i,j} = O(\epsilon^{2/3}), \quad N+1 \leq i+j \leq 2N, \\ \beta_{i,j} &= O(\epsilon), \quad 2N+1 \leq i+j \leq 3N. \end{aligned} \right\} \quad (3.8)$$

Note, that although the two asymptotics (3.7) and (3.2)+(1.2) include the relationships for σ , the derivation of the adaptive modal systems, as it occurs in the modal modelling, does not link σ and ϵ (see the special discussion on this by Faltinsen *et al.* 2000; Faltinsen & Timokha 2001). The adaptive modal system based on (3.8) is easily derivable from (2.1) by accounting for (3.8) and keeping the terms of $O(\epsilon)$. It has $N(N+3)/2$ dominating modes and the size dimension $9N(N+1)/2$. Increasing N yields a series of ‘embedding’ adaptive modal systems, where the case $N = 1$ corresponds to the modal theory considered in Part 1. When $N \geq 3$, all the nine lowest modes from the model in Part 1 are considered by the adaptive modal system to be dominating ones. However, if the actual steady-state solutions are consistent with the asymptotic ordering of Part 1, their numerical approximation obtained with the adaptive system for $N \geq 3$ should give an error $o(\epsilon)$ which is negligible in our asymptotic analysis. When accounting for another type of solution based on (3.7), this point gives a ‘convergence’ criterion for the adaptive modal modelling which suggests two steps: (i) The condition (3.5) indicates amplification of the modes $i+j=2$ and a switch to the adaptive models with $N \geq 2$. (ii) The smallness of the difference (in scale $\epsilon^{1/2}$) between numerical results of the adaptive modal systems obtained with N

and $N + 1$ indicates that the actual dimension of the dominating modes from (3.7) is N .

The requirement to test different $N \geq 2$ may cause numerical stiffness for subsystems corresponding to the higher modes. The problem can be slightly relaxed because the modal functions $\beta_{i,j}$, $2N + 1 \leq i + j \leq 3N$, are $o(\epsilon)$ for both asymptotics with increasing N and can often be omitted in the numerical analysis. However, $\beta_{i,j} = O(\epsilon)$, $N + 1 \leq i + j \leq 2N$, are theoretically unavoidable for steady analysis and play an important role for transient regimes. Calculations of transient waves without those higher-order modal functions sometimes gave results in numerical tests that are far away from reality and even resulted in numerical instability. The physical explanation is that, while the lowest-order modes determine a global ‘smooth’ fluid flow, the higher-order modes are responsible for modelling short steep waves. These waves always appeared in the experiments and cannot be excluded from consideration. However, the experiments also confirmed that these waves have a very short life due to various dissipative factors including probably surface tension, local breaking and so on.

Mathematically, the structure of the modal equations for $\beta_{i,j}$, $N + 1 \leq i + j \leq 2N$, is as follows:

$$\ddot{\beta}_{i,j} + 2\alpha_{i,j}\dot{\beta}_{i,j} + \sigma_{i,j}^2\beta_{i,j} = F_2(\beta_{l,m}), \quad N + 1 \leq i + j \leq 2N, \quad 1 \leq l + m \leq N. \quad (3.9)$$

These equations are linear in $\beta_{i,j}(t)$, $N + 1 \leq i + j \leq 2N$, and the right-hand side F_2 is a quadratic function of the dominating modal functions and their derivatives. The modal functions $\beta_{i,j}(t)$, $N + 1 \leq i + j \leq 2N$, are also linearly present in the equations for these dominant modes $\beta_{l,m}(t)$, $l + m \leq N$. Due to the linear structure of (3.9), the high-frequency components in solutions of (3.9) will then depend exclusively on either initial conditions or numerical time integration errors. Dissipation rates in the higher equations (3.9) are not predicted well by (2.4) + (2.5) and therefore their usage, especially for transients, may result in numerical solutions of $\beta_{i,j}(t)$, $N + 1 \leq i + j \leq 2N$, with magnitudes larger than magnitudes of dominating modes and lead to conflicts in our asymptotic scheme. Thus, two principal problems of the adaptive scheme are to find a strategy for damping of the higher-order modes and to estimate the initial conditions.

When the steep wave profiles and local breaking waves do not occur, dissipative features of the hydrodynamic system are mostly related to viscous damping in the dominating (lowest-order) modes (Hill 2003). However, the values (2.4) + (2.5) represent only a lower bound of dissipation for higher modes. This point and the previously mentioned numerical problem for equations (3.9) lead to the following strategy for handling the damping: (i) the prediction (2.4)–(2.5) is only used for the dominating modes $i + j \leq N$; (ii) the second-order modes $i + j \geq N + 1$ are critically damped, i.e. $\alpha_{i,j} = \sigma_{i,j}$; (iii) the tested dimensions are restricted by $N \geq 2$.

Physically, the strategy provides the viscous damping rates for the lowest-order modal functions and guarantees that at least the nine lowest modal functions appearing in Part 1 are damped with (2.4) and (2.5). Short waves due to the second-order modal functions are damped with the much larger critical rates. The error caused by using the critical damping as an estimate affects only the higher-order contribution of $O(\epsilon)$ in steady-state wave regimes. Indeed, when periodic solutions are consistent with the Narimanov–Moiseyev asymptotics, the critical damping is applied to the modes $\beta_{i,j}(t) \leq O(\epsilon)$, $i + j \geq 4$, which either are absent in the lower-order equations or contribute $o(\epsilon)$ to them. If steady-state solutions are consistent with (3.7), the critical damping terms appear only in the equations of the second-order modes that are of $O(\epsilon)$ and contribute only $o(\epsilon)$ to the equations of the dominating

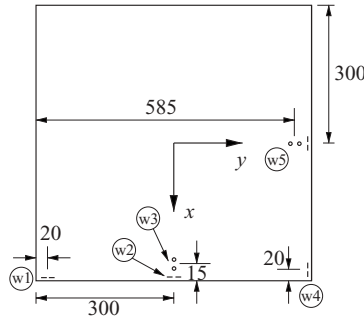


FIGURE 2. Positions w_i of the wave probes (tank seen from above). Measurements in mm.

modes $i + j \leq N$. The maximum error in approximating the steady-state motions is therefore of $O(\epsilon)$. Another problem is associated with the damping rates (2.4) and (2.5) in the equations of the lowest-order modes. Since they provide only a lower bound of the actual dissipation, the use of (2.4) + (2.5) prevents us from testing large-dimensional adaptive systems. Our computational experiments show that modal systems are numerically stiff for $N \geq 6$ for three-dimensional resonant waves related to our experimental series.

While our damping strategy does not influence the lowest-order component of steady-state solutions, it may in general fail for transient waves, when the actual dissipation of lower/higher modes is re-distributed in a different way and other physical phenomena such as local breaking may matter. This motivated us to focus also on transient regimes in the validation of this approach.

As shown in Part 1, three-dimensional resonant sloshing in a square-base basin is characterized by multiple steady solutions for the same forcing frequency. Initial conditions therefore play an important role in determining both the actual steady-state motion and transient phase. A particular example is that zero initial conditions for longitudinal forcing lead always to planar motions and the transition to swirling and chaotic motions cannot be described. Our strategy for finding appropriate initial perturbations in the system uses the experimental measurements at wave probes 3 and 5 (see figure 2) during approximately two times the largest natural periods prior to forced oscillations of the tank. The small wave elevations can then be described by linear theory and a Fourier analysis in this time range provides estimates of the initial conditions for $\beta_{i,j}$. Numerical experiments showed that the estimates of the higher modes were sufficiently small and do not affect the behaviour during forced sloshing. Only initial perturbations of the two lowest modes $\beta_{1,0}$ and $\beta_{0,1}$ matter, while zero initial conditions may be accepted for the higher modes.

4. Model tests and validation

4.1. Experimental setup and observations

The model tests were performed in a cubic tank with dimensions 0.6 m. The tank structure was made of 20 mm thick acrylic with a steel frame added for support. The weight of the empty tank and frame is 124 kg. The measurements are within 1 mm of the given values, the tank model is horizontal within 0.5° . The instrumentation consists of wave probes, force gauges, accelerometers, steering system velocity feedback monitoring and a digital video camera. Only the two wave probes labelled w3 and w5 in figure 2 are used in this study. Two lengths of parallel wire separated by 10 mm

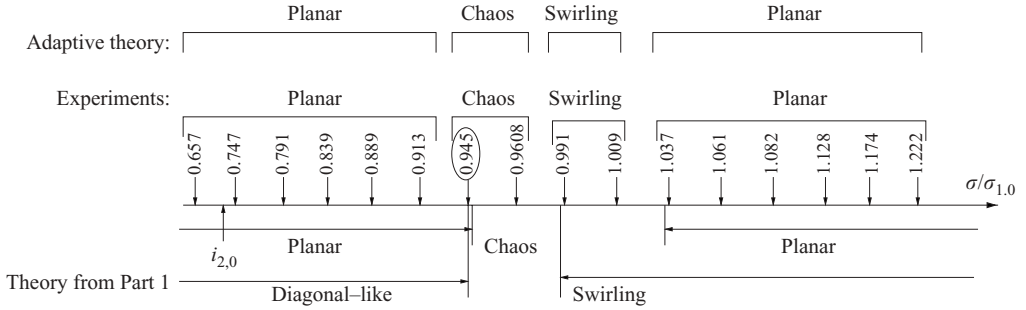


FIGURE 3. Longitudinal forcing with $h = 0.5$, $\epsilon = 0.00817$. Comparison between experimental data, theoretical prediction from Part 1 and results of the adaptive modal theory.

are stretched vertically between the tank bottom and roof. Four force gauges referred to as guide towers support the frame enclosing the tank model. Each guide tower includes three strain gauges to facilitate force measurements along all three axes. The accelerometers are aligned with the x - and y -axes and are situated on top of the tank model. These are used to measure the exact tank motion, and are a supplement to the measured servo-motor velocity from the feedback steering system. Most test runs last 5 minutes. The data analysis is performed in Matlab. A filtering frequency of 5 Hz is applied for both forces and accelerations when accelerometer readings are used to calculate the horizontal forces, excluding the inertia force due to tank mass. The peak period from a spectral analysis of the tank motion provides the exact forcing frequency. A special damping device was used to reduce the time between each test. A horizontal mesh of metal was lowered onto and through the free-surface to suppress the free-surface motion.

Pure periodic waves were not detected even after 270–350 forcing periods. Both wave elevation and hydrodynamic force amplitudes demonstrated fluctuations of up to 5–30% (depending on the type of wave regime). The experiments re-confirmed conclusions in Part 1 including the classification of nearly-periodic waves. The steepness of the wave pattern and local breaking phenomena were predominating for three-dimensional regimes. They appeared as sheets of water (run-up) being ejected up the tank walls as well as more localized vertical jets of a very limited spatial extent. The run-up has a strong three-dimensional flow character even when the flow at a small distance from the walls is mainly two-dimensional. The thin sheet of water ejected upwards collapses, scatters and the water falls down on the free surface like ‘rain’ covering a small part of the free surface area. The run-up process may end the pure two-dimensional nature of the flow and trigger three-dimensional flows like diagonal or swirling waves. Such a ‘rainfall’ was repeated each $1/4$ of the forcing period for nearly periodic waves, but involved statistically different fluid volumes.

4.2. Longitudinal forcing

Figure 3 shows an experimental and theoretical classification of wave regimes after the transient phase for $h = 0.5$, $\epsilon = 0.00817$. While the theoretical results in Part 1 are obtained analytically from the corresponding bifurcation analysis, the frequency domains of the adaptive systems are determined by looking at the numerical solutions of the approximate equations. Comparing the results from the Part 1 system, we find qualitative agreement except for $\sigma/\sigma_{1,0} = 0.9455$, where the experiments show chaotic motions instead of planar waves. Moreover, except for the cases with $\sigma/\sigma_{1,0} = 0.9455$ and 1.037 , the planar regimes are in good quantitative agreement with Part 1 for

both wave elevation near the walls and the hydrodynamic forces. This is so even for $\sigma/\sigma_{1,0} = 0.657$ and 0.747 , which are close to $i_{2,0} = 0.73 \dots$ (the prediction of the secondary resonance in the asymptotic limit $\epsilon \rightarrow 0$). This resonant zone is probably too narrow for our ϵ . In contrast to Part 1, the results by the adaptive model agree well for all the experimental series.

Since the experimental series with three-dimensional wave regimes demonstrate significant local phenomena (see §4.1) after 8–12 forcing periods and there is not a clear theoretical strategy in dealing with perturbations caused by local phenomena, the validation was divided into two cases: (i) a description of the initial transient phase, when these perturbations still do not influence the sloshing and (ii) a classification of nearly steady-state waves by performing very long time calculations. The number of dominating modes in the adaptive scheme was detected to be $i + j \leq N = 3$ to handle both transient and nearly periodic waves. Using a larger N up to $N = 6$ gave small differences (up to 1–4%). The initial conditions strategy confirmed in general its applicability for the adaptive modal systems. While the numerical results for $N \geq 3$ were not sensitive to small changes in the initial conditions, the modal system in Part 1 led to numerical breakdown for the experimental cases observing three-dimensional motions. Only long-time-domain simulations (200–300 forcing periods) with $N = 6$ showed a slightly increasing numerical error caused probably by stiffness. A possible reason is that our linear viscous estimate of the damping (2.4), (2.5) for $\beta_{i,j}$, $i + j = 6$ does not reflect the real dissipation in the system.

The adaptive method computes $N = 3$ for non-swirling waves with $\sigma/\sigma_{1,0} = 0.945$, 0.9608 and 1.037 and generally agrees well with experiments for both the initial transient phase (approximately 15–20 forcing periods) and nearly steady regimes. Extensive comparisons suggested that future research should consist of modelling random-like perturbations generated by the local phenomena. Neglecting them in the numerical analysis does not allow quantitative theoretical predictions in the ‘intermediate’ transient phase, namely immediately after the initial transients.

Figure 4 shows results for $\sigma/\sigma_{0,1} = 1.037$. While numerical results agree well with experiments for both initial transients (for approximately $t \leq 12$ s in figure 4*a–d*) and nearly steady waves (after approximately 100 s), the intermediate time range exhibits clear disagreement. Since the local phenomena affect elevations near the walls, we were able to show in figure 4(*e, f*) how they (see the ellipses) drive the discrepancy between measured and computed elevations after 12 s. Another series with $\sigma/\sigma_{0,1} = 0.9608$ is characterized by the predominating character of the random-like perturbations. The transition to chaotic motions was in this case associated with a short-life swirling. Although the calculations in figure 5(*a–d*) capture qualitatively these transients after 10–12 s, the initial condition strategy always results in the transient swirling in the opposite direction to those observed in experiments. This can be established by studying the shift of the peaks for the wave elevations in the time domain 15–26 s. The reason is that the initial conditions in this case are very small relative to those in other experimental series. While the larger initial conditions imply a predominating influence of the initial perturbation on the initial transient phase, the measured elevations at probes 3 and 5 in the last case were comparable with the static capillary meniscus at the wave probes and both the surface tension and the local phenomena may be important for the initial transients.

Special effort was made to improve the theoretical prediction at $\sigma/\sigma_{0,1} = 0.9455$, where Part 1 disagreed with experiments. While $N = 1$ and 2 always led to two-dimensional sloshing, the adaptive method with $N \geq 4$ confirmed the ‘chaotic’ character of the sloshing in very long time series (we tested up to 1000 s). The final results for

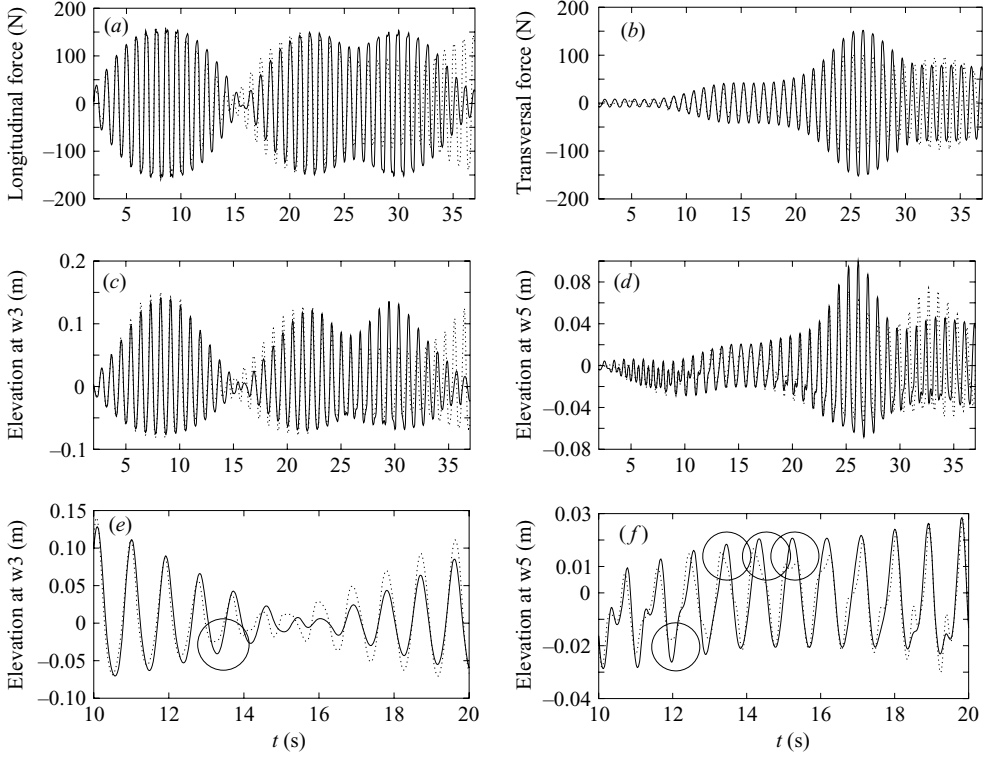


FIGURE 4. Transient waves. Longitudinal forcing with $h = 0.5$, $\epsilon = 0.00871$ and $\sigma/\sigma_{1,0} = 1.037$. The solid line presents the calculations by the adaptive modal system and the dashed line gives the measured data for longitudinal/transversal forces (a, b) and wave elevations at wave probes 3 and 5 (c, d) (see figure 2). (e, f) Zoomed time history after $t = 14$ s, which confirms the presence of the short-time perturbations, most probably caused by local near-wall phenomena.

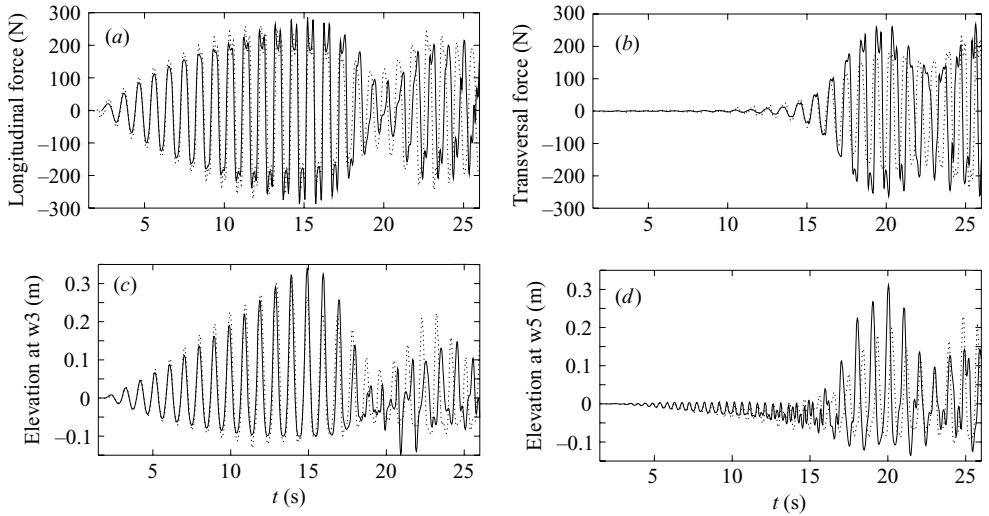


FIGURE 5. The same as in figure 4(a–d), but with $\sigma/\sigma_{1,0} = 0.9608$.

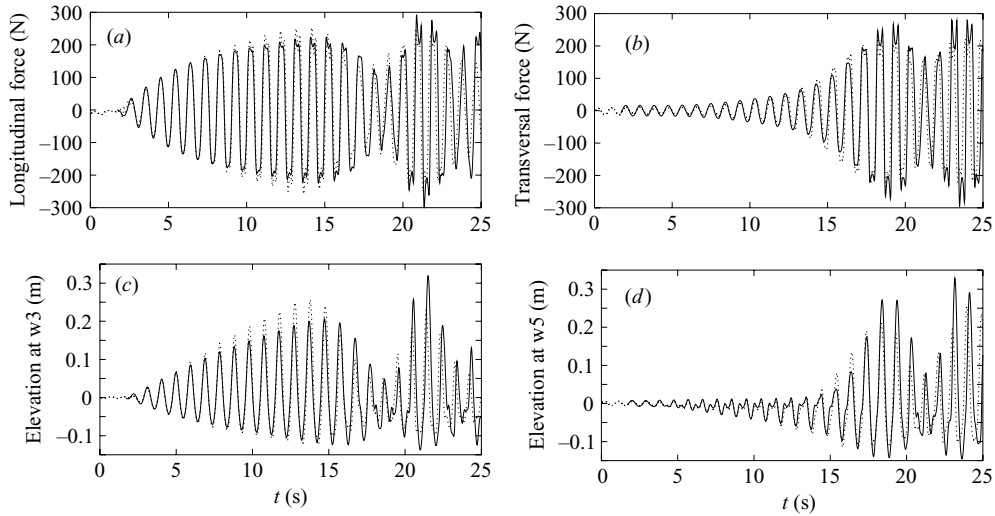


FIGURE 6. The same as in figure 4(a–d), but showing the transition to ‘chaotic’ wave motions for $\sigma/\sigma_{1,0} = 0.945$.

the three-dimensional transients are also illustrated in figure 6(a–d). The agreement is especially good for the forces, but the wave elevation after approximately 10 s is affected by the local phenomena (§4.1).

Theoretical results for transient waves leading to swirling regimes are also affected by the local phenomena, but agree well with experimental measurements beginning from $N=3$. This is exemplified for $\sigma/\sigma_{0,1} = 1.009$ in figure 7(a–f). Note, that although nearly steady-state swirling regimes are identified in the two experimental cases detecting the swirling regimes, the measurements do not show pure periodic waves. The measurements at wave probes 3 and 5 were always affected by random-like fluctuations of up to 10–30% of the maximum wave elevations. Since the hydrodynamic forces depend basically on the dominating modes, the measured hydrodynamic forces in these cases demonstrate more clearly a nearly periodic behaviour. We performed some additional numerical studies of long time series using our adaptive scheme to compare theoretical and experimental results in the steady-state regimes. Some numerical results are illustrated in figures 8 and 9.

The first example in figure 8 confirming applicability of our adaptive scheme is for $\sigma/\sigma_{0,1} = 1.009$ (the last part of the experimental time history was studied). The beating in the numerical results did not die out even after 1000 forcing periods. An explanation is that the predictions of linear viscous damping in the lowest-order modes do not account for the actual dissipation in this case. An opposite physical situation related to $\sigma/\sigma_{0,1} = 0.991$ is presented in figure 9(a–d). Although the applicability of the adaptive asymptotics is also justified in this case and short transients led to nearly periodic solutions that agreed with experiments (see figure 9a,b), the comparison for larger t in figure 9(c,d) demonstrates a disagreement. The discrepancy did not depend on the value of $N \geq 3$. The damping is probably estimated well, but the random-like perturbations play a much more important role. A speculative study of this hypothesis was made by perturbing some higher modal function $\beta_{i,j}(t) = o(\epsilon)$, $N+1 \leq i+j \leq 2N$ at an instant $t=t_0$. Although these perturbations were lower than the error of our asymptotic scheme, they led after short transients (up to 3–5 forcing periods) to a situation similar to that in figure 9 (a,b).

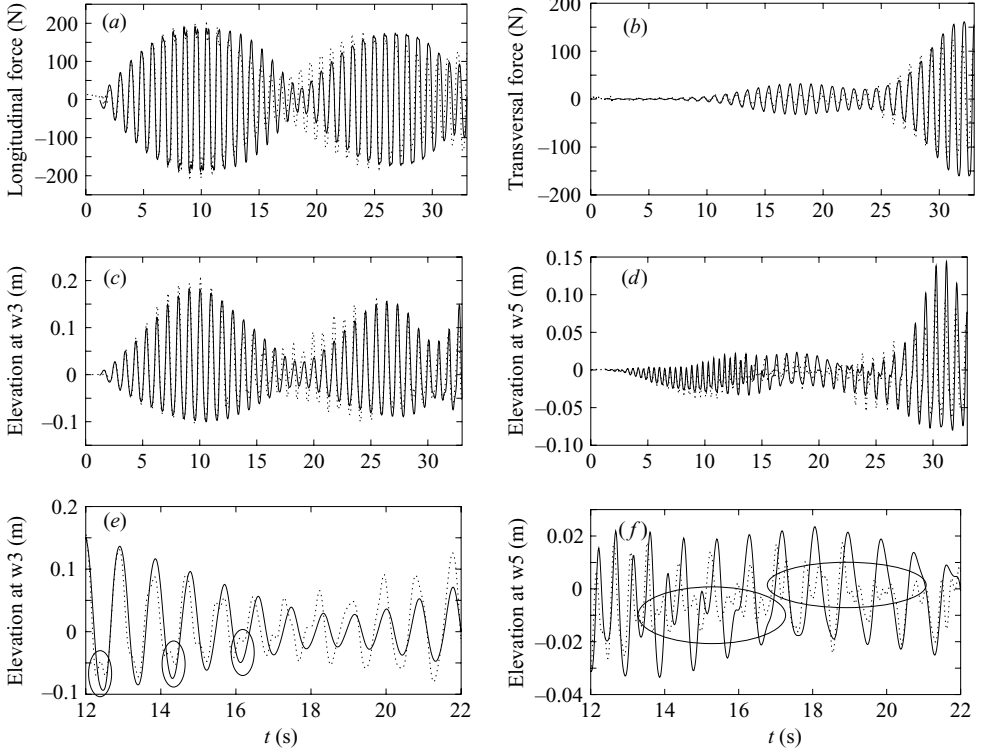


FIGURE 7. The same as in figure 4, but showing the transition to swirling waves with $\sigma/\sigma_{1,0} = 1.009$. (c,d) Zoomed time history after $t = 12$ s, which confirms the presence of random-like perturbations caused by the local phenomena (§4.1).

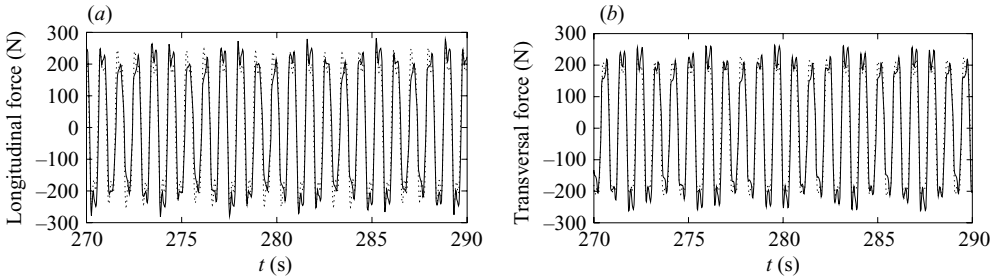


FIGURE 8. The same as in figure 7(a,b), but for nearly periodic waves.

4.3. Diagonal forcing

Figure 10 shows a comparison of wave regimes after the transient phase predicted by adaptive theory, experiments and the theory in Part 1 in the case of diagonal forcing. The theory in Part 1 gives in many cases satisfactory predictions. However, comparing experimental data and predictions from Part 1 shows unsatisfactory predictions when $\sigma/\sigma_{0,1} = 0.929, 0.94575, 0.973, 1.022$ and 1.115 . The adaptive approach improved the theoretical results and confirmed indirectly that amplification of higher modes may affect the qualitative classification of steady regimes relative to the Narimanov–Moiseyev scheme (Part 1; Faltinsen *et al.* 2004). The numerical results are in especially good agreement with the experiments showing stable diagonal sloshing. An example

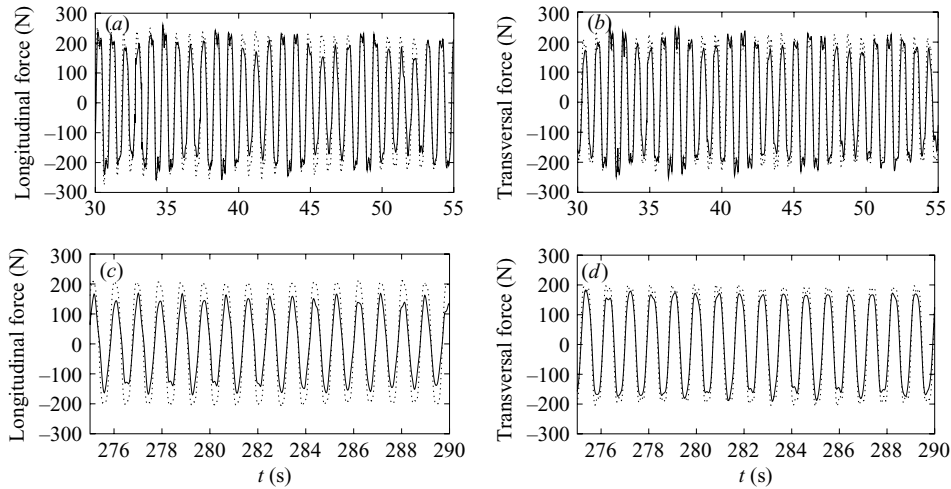


FIGURE 9. The same as in figure 8, but for $\sigma/\sigma_{0,1} = 0.991$, shown in (a, b) at an early time.

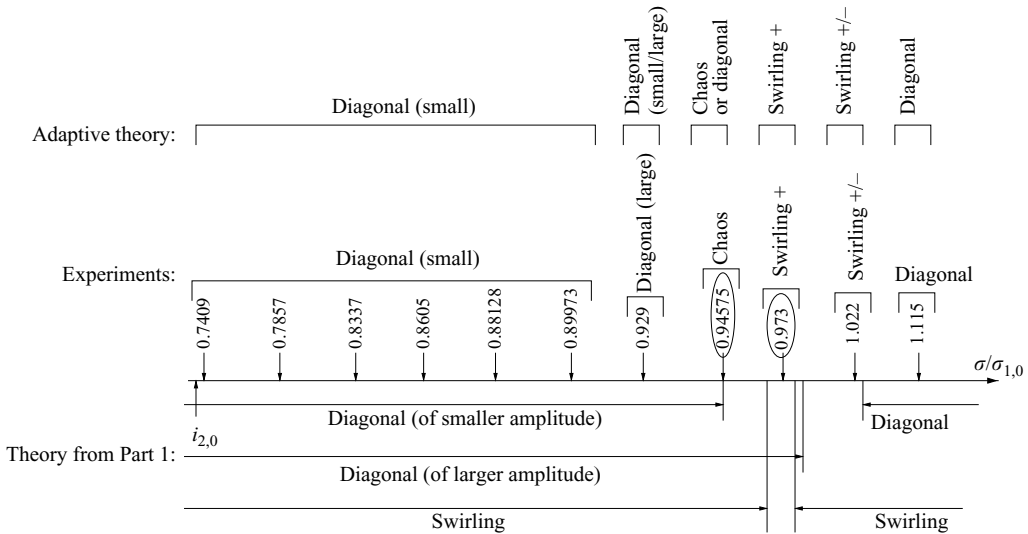


FIGURE 10. The same as in figure 3, but for diagonal forcing.

illustrating calculated and measured transient waves in the initial phase is presented in figure 11(a–d).

Experimental swirling waves for $\sigma/\sigma_{1,0} = 1.022$ show a repeated switching of the rotation direction. This is a kind of ‘beating’, which was not observed for longitudinal forcing, but it is well known from experimental studies on swirling motions in circular and spherical tanks. In particular, Abramson (1966, p. 99) writes on swirling regimes in a spherical tank: ‘... The motion is even more complicated as a type of ‘beating’ also exist; the first antisymmetric liquid-sloshing mode first begins to transform itself into a rotational motion increasing in angular velocity in, say, the counterclockwise direction, which reaches a maximum and then decreases essentially to zero and then reverses and increases in the clockwise direction, and so on alternatively.’ Time recordings of the wave elevations and hydrodynamic forces in square-base tank show that, in

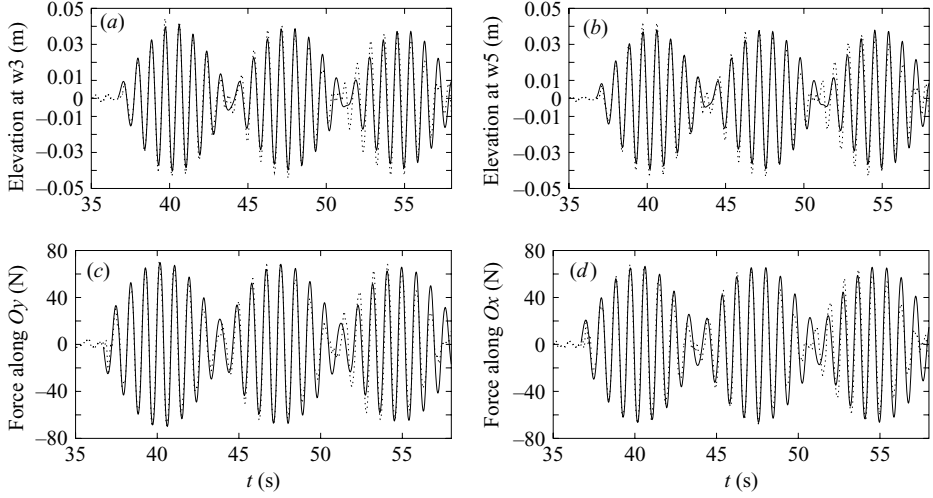


FIGURE 11. Measured (dashed line) and calculated (solid line) wave elevations (a,b) and hydrodynamic forces (c,d) by the adaptive modal system for the initial transient phase in the case of diagonal forcing with $\sigma/\sigma_{1,0} = 1.115$, $h = 0.5$, $\epsilon = 0.00871$.

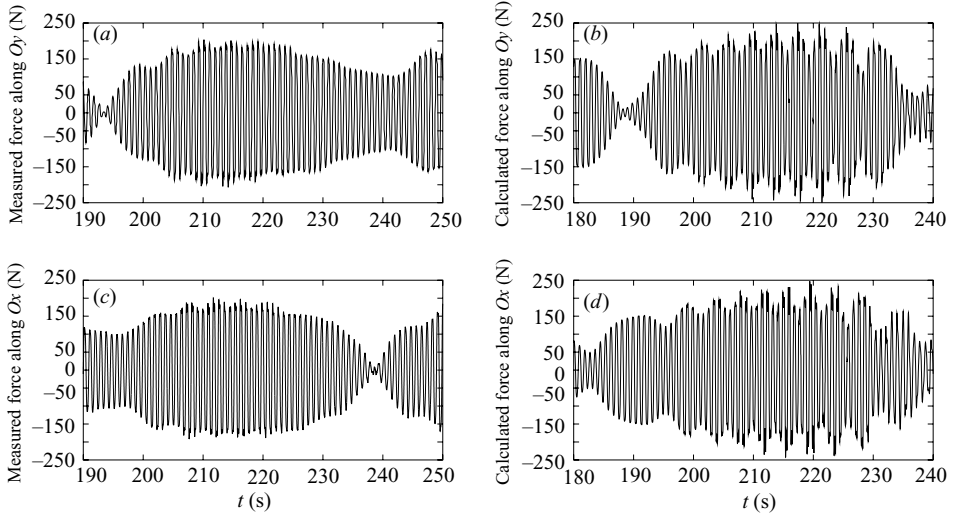


FIGURE 12. Measured (a,c) and calculated (b,d) wave elevations for $\sigma/\sigma_{1,0} = 1.022$.

contrast to swirling regimes in spherical tanks, the switching is most probably affected by random perturbations occurring due to the local phenomena (§4.1). Although our adaptive modal scheme does not account for these perturbations, it captures the switching. The numerical perturbations are due to small errors in approximating higher modes. While the simplest modal system in Part 1 does not capture this phenomenon at all (it simply fails for this forcing), the adaptive model describes it qualitatively well. Figure 12 gives typical measured and calculated ‘beating periods’.

Another set of physical phenomena is associated with the experimental case $\sigma/\sigma_{1,0} = 0.973$. Experiments clearly demonstrate a swirling wave of fixed rotation direction with only small ‘beating’. Since the forcing frequency belongs to a narrow

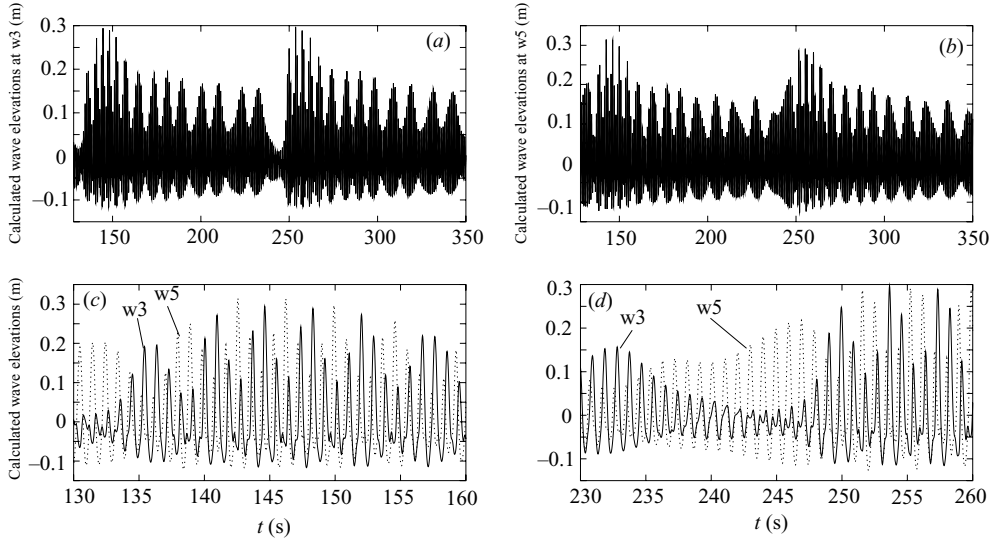


FIGURE 13. Calculated regular beating by the adaptive modal system. Wave elevations at probes 3 and 5 (see figure 2) in a test case of diagonal forcing with $\sigma/\sigma_{1,0} = 0.973$, $h = 0.5$, $\epsilon = 0.00871$.

zone between two Hopf bifurcation points (Part 1 p. 25), the swirling wave is theoretically unstable for this forcing frequency in the framework of the Narimanov–Moiseyev asymptotics, which predicts here only stable steady-state diagonal wave of large energy (amplitude). However, as remarked in Part 1 on p. 26, even a relatively small dissipation might stabilize the swirling waves. We performed numerical studies of this case by use of the adaptive modal scheme to try to estimate N , initial conditions and even to change them speculatively. However, although the initial transient phase has been quantified well, significant beating in numerical solutions made it impossible to identify the actual periodic motions as precisely as in the experiments. Depending on initial conditions long-time simulations represented surprisingly regular structures (see examples in figure 13*a, b*). Although the numerical periodic solutions were not found, the calculated series were classified as a swirling wave with constant direction of rotation. This is illustrated in figures 13(*c, d*) by comparing the computed wave elevation at wave probes 3 and 5. They show clearly a fixed phase difference of one-fourth of the excitation period between peaks at probes 3 and 5 (see the identification method in Part 1).

Finally, the experiments with $\sigma/\sigma_{1,0} = 0.94575$ indicate clearly ‘chaotic’ surface wave motions, while the theoretical prediction by the Narimanov–Moiseyev asymptotics consists of two stable steady-state diagonal waves (of lower and smaller amplitudes) and a stable swirling regime (in fact, two more regimes, because of two possible direction of rotation). Trying to identify the actual steady solution with our adaptive modal scheme and suitable initial conditions always showed a diagonal wave of lower amplitude. This stable regime has lower energy than other possible stable regimes and our calculations lead to this regime with sufficiently small initial conditions. ‘Chaotic’ waves in the experiments are probably caused by additional perturbations in the system occurring due to local phenomena (§4.1). Since these perturbations are not accounted for by our model, they can only be modelled by increasing the initial conditions relative to our initial conditions strategy. Doing this by a factor 3 we

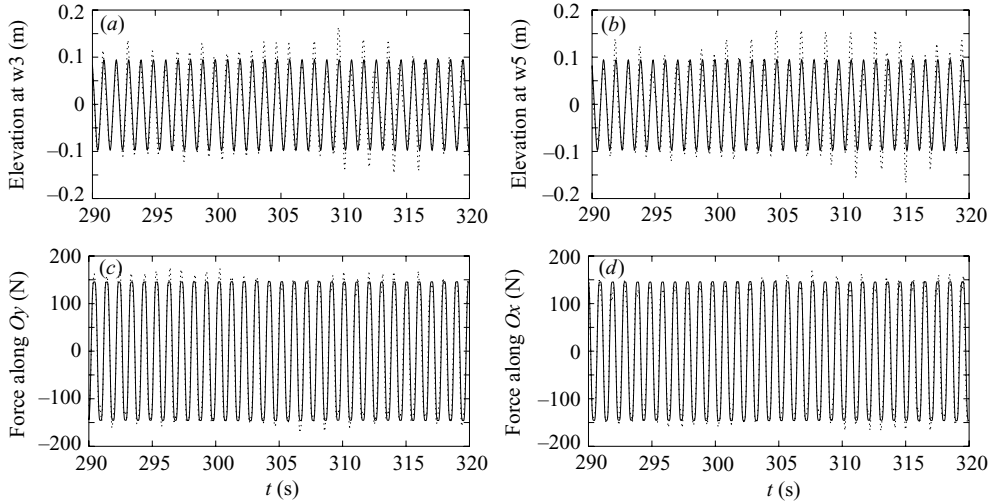


FIGURE 14. The same as in figure 11, but for $\sigma/\sigma_{1,0} = 0.929$.

found a ‘chaotic’ resonant wave response, which did not die out for very long time (up to 3000 forcing periods were tested). The importance of random-like perturbations during sloshing is also demonstrated for the experimental case $\sigma/\sigma_{0,1} = 0.929$. Here both the experiments and our adaptive theory identify two steady-state diagonal solutions. However, the experiments showed the diagonal wave of larger amplitude, while calculations based on predicted initial perturbations led to diagonal waves of lower amplitude. Only large increases in initial perturbations relative to experimental estimates and usage of the adaptive scheme (the Narimanov–Moiseyev asymptotics simply fails to compute this case) made it possible to obtain the same nearly steady-state regime as in the experiments. Theoretical and experimental results agree well (see the comparison in the last seconds of the experimental test in figure 14a–d). The agreement is better for hydrodynamic forces in figure 14(c, d), while wave elevations in figure 14(a, b) show significant effects of random perturbations due to local breaking at the corners.

5. Conclusions

We suggested in Part 1 that the discrepancy between experiments and theoretical asymptotic results of steady-state resonant sloshing in a square-base tank with finite fluid depth may be due to amplification of higher modes caused by secondary resonance. This hypothesis was based on both experimental observations of steep (short) three-dimensional wave profiles accompanied by numerous local breaking phenomena and theoretical quantification of a similar discrepancy for two-dimensional resonant sloshing in a rectangular tank occurring for relatively large sway/roll forcing amplitude (Faltinsen & Timokha 2001). Further analysis of experimental data showed that the concept of secondary resonance in Faltinsen & Timokha (2001) is not applicable in our case. The present paper gives a new theoretical analysis of the amplification by proposing a new version of an adaptive modal approach capturing a selective (depending on the type of motions) secondary resonance in higher modes. The theoretical basis of the adaptive approach is a generic infinite-dimensional modal system which played an auxiliary role in the

previous paper. New experimental studies have been done to re-confirm experimental conclusions of the previous paper and provide longer time records of measurements.

The new concept of secondary resonance and quantification of amplification of higher modes is based on comparing the contributions from second-order and dominating modes. It is developed for steady-state motions, but one part of the validation is associated with transient regimes. An exact analytical result (necessary condition (3.5)) is derivable only for the second-order modes in terms of the model in Part 1, i.e. $\beta_{i,j}, i + j = 2$. Since the asymptotic condition (3.5) depends on the actual lowest-order contribution varying along the response curves, the amplification of $\beta_{i,j}, i + j = 2$, depends strongly on the type of steady wave regime. This clarifies the selective effect for higher modes observed in the experiments and makes it possible to quantify the actual frequency domain where the third-order Narimanov–Moiseyev asymptotic scheme becomes invalid and the number of dominating modes increases. This needs a new asymptotic ordering matching the second-order terms to $O(\epsilon)$. It is straightforward, but analytically very tedious, to derive the asymptotic conditions analogous to (3.5) for $i + j \geq 3$. Another problem consists of combining two asymptotics to describe planar waves (in the framework of the Narimanov–Moiseyev ordering) and three-dimensional steady motions (with the new ordering) simultaneously by a single modal system. This is an important problem for transient waves, implying a possible switch between different wave regimes. The present paper proposes an adaptive scheme allowing detection of the actual number of dominating modes and derives a finite-dimensional model including the nonlinear terms required by both asymptotics. The existence of two different asymptotics for the same forcing parameters requires further analytical studies. Our main focus was to validate our theoretical quantification of amplification and prove the physical hypothesis in Part 1. Several cases were described where the simplest modal system in Part 1 failed, but the adaptive modal scheme predicts the steady-state motions well and agrees with measured data. Although our theory has been confirmed by comparing with earlier and new experiments, the adaptive scheme, and the modal methods in general, are found to be limited by their ability to model local phenomena and also damping of higher-modes.

The adaptive modal systems need to include realistic damping to describe transition to steady-state motions. Our way of approximating the damping assumes linear viscous damping rates for the dominating modes and critical damping for the second-order modes. The critical damping in the second-order modes influences only higher-order components of steady-state motions solutions and may affect only some special sort of transient. Intuitively, it is responsible for short-life steep wave patterns and dissipation due to overturning waves. In contrast, the linear viscous damping rates imply a lower limit of dissipation in the lower-order modes and may become too small for large N ($\beta_{i,j}(t), i + j = N$). The error in neglecting dissipation due to local phenomena for the dominating modes should be studied further. This requires both an estimate of the energy loss due to breaking waves and its redistribution between the natural modes. However, both our damping strategy and even the higher modes amplification may imply the greatest effect where the full formulation associated with inviscid potential flows breaks down anyway. With increasing forcing amplitudes we reach the situation when many modes should formally be considered of dominating order, but many of them are affected by various kinds of damping including local phenomena. Such wave motions require not only other methods, but probably a physical formulation that allows for a rotational flow.

While the conclusion regarding damping is similar to that made by Faltinsen & Timokha (2001) for two-dimensional waves, a new finding is that local phenomena cause random-like perturbations. Since in many cases at least two steady-state solutions exist (an example is swirling with opposite rotation directions), these perturbations can change the stability features of steady-state sloshing. Experiments show that they may cause transition to chaotic motions in the frequency domain where several stable steady-state solutions exist. All these cases are captured by our adaptive modal scheme however, but a strategy is needed for modelling these random perturbations over long-time simulations. Perturbation effects of local phenomena need to be addressed by a modal method and any other (including CFD) scheme for three-dimensional sloshing in a prismatic tank.

A.N.T. gratefully acknowledges the support of the Alexander-von-Humboldt Foundation (Germany) and the Centre for Ships and Ocean Structures at NTNU (Norway) in funding the work described here.

REFERENCES

- ABRAMSON, H. N. 1966 The dynamics of liquids in moving containers. *NASA Rep.* SP 106.
- BRYANT, P. J. 1989 Nonlinear progressive waves in a circular basin. *J. Fluid Mech.* **205**, 453–467.
- FALTINSEN, O. M., ROGNEBAKKE, O. F., LUKOVSKY, I. A. & TIMOKHA, A. N. 2000 Multidimensional modal analysis of nonlinear sloshing in a rectangular tank with finite water depth. *J. Fluid Mech.* **407**, 201–234.
- FALTINSEN, O. M., ROGNEBAKKE, O. F. & TIMOKHA, A. N. 2003 Resonant three-dimensional nonlinear sloshing in a square-base basin. *J. Fluid Mech.* **487**, 1–42 (referred to herein as Part 1).
- FALTINSEN, O. M., ROGNEBAKKE, O. F. & TIMOKHA, A. N. 2004 Classification of three-dimensional nonlinear sloshing in a square-base tank with finite depth. *J. Fluids Struct.* (in press).
- FALTINSEN, O. M. & TIMOKHA, A. N. 2001 Adaptive multimodal approach to nonlinear sloshing in a rectangular tank. *J. Fluid Mech.* **432**, 167–200.
- GAVRILYUK, I., LUKOVSKY, I. A. & TIMOKHA, A. N. 2000 A multimodal approach to nonlinear sloshing in a circular cylindrical tank. *Hybrid Meth. Engng* **2**, 463–483.
- HILL, D. F. 2003 Transient and steady-state amplitudes of forced waves in rectangular tanks. *Phys. Fluids* **15**, 1576–1587.
- LA ROCCA, M., MELE, P. & ARMENIO, V. 1997 Variational approach to the problem of sloshing in a moving container. *J. Theor. Appl. Fluid Mech.* **1**, 280–310.
- MOISEYEV, N. N. 1958 To the theory of nonlinear oscillations of a limited liquid volume of a liquid. *Prikl. Mat. Mech.* **22**, 612–621 (in Russian).
- NARIMANOV, G. S. 1957 Movement of a tank partly filled by a fluid: the taking into account of non-smallness of amplitude. *Prikl. Mat. Mech.* **21**, 513–524 (in Russian).